Seafloor Alteration Governed by Oceanic Crustal Age and Redox Conditions: Insights from Machine Learning-based Elemental Transfer Analyses

Satoshi Matsuno[1*], Masaoki Uno[1*], and Atsushi Okamoto[1]

[1] Graduate School of Environmental Studies, Tohoku University, Japan

Corresponding author: Satoshi Matsuno (satoshi.matsuno.p2@dc.tohoku.ac.jp), Masaoki Uno (masa.uno@tohoku.ac.jp)

Key Points:

- This study introduces a new approach for quantitatively analyzing element mobility in altered basaltic crusts using a regional dataset.
- Findings indicated that older altered basalts had higher element mobility, with variances linked to the redox state of the environment.
- Sediment thickness is a key determinant of redox condition during seafloor alteration and affects element transfer and mineral formation.

Abstract

Newly formed oceanic crust interacts with penetrating seawater, resulting in the formation of secondary minerals. Sediment cover can potentially change the redox conditions of underlying basaltic crusts, significantly affecting the types of secondary minerals and element transfer during alteration. However, previous studies have not revealed the quantitative regional variation and controlling factors of seafloor alteration using altered samples taken from different sites. We present a novel approach for the quantitative analyses of element mobility related to seafloor alteration based on a regional dataset of altered basalt bulk compositions and highlights the effects of the redox state and duration on alteration. The protolith reconstruction models (PRMs), machine learning-based element mobility analyses, were applied to the compositional data of the basaltic crusts from the South/Northwest Pacific region. The analyses revealed that altered basalts with older ages showed higher element mobility, particularly characterized by an enrichment of Rb and K, which were associated by up to 100 times with the formation of secondary minerals. In the oxidative settings of the South Pacific region, enrichment of Ba, U, and Pb and depletion of P were observed in samples with intense alteration. In contrast, under reductive conditions in the Northwest Pacific region, alterations associated with carbonate veins caused U enrichment. Our research suggests that sediment thickness is a key factor in the redox conditions during alteration, which changes the characteristics of element transfer and secondary minerals. Additionally, seafloor alteration likely persisted for at least 30 Myr, irrespective of whether the environment was oxidative or reductive.

Plain Language Summary

When the oceanic crust is altered with seawater, it involves the formation of new minerals and the transfer of various elements over time. However, methodological limitations have made it challenging to distinguish the original compositional character from the alteration process, posing an obstacle to the quantitative analysis of regional variations and the controlling factors of alteration. To overcome this limitation, we employed new element mobility analyses using a machine learning approach and examined samples from different regions of the Pacific Ocean, each exhibiting distinct characteristics, such as sediment thickness and age. Our study discovered that the older the oceanic crust, the more pronounced the changes in elemental mobility. In addition, the elements that undergo mobility are influenced by the redox condition controlled by the sediment thickness on the oceanic crust, changing the formation of alteration minerals and specific element mobility. Our study is the first to quantitatively demonstrate the effects of crust ages, redox conditions, and sediment thickness on the element mobility, suggesting that these alterations in the ocean floor can persist for over 30 million years. This research enhances our understanding of the long-term evolution of Earth's oceanic crust and the composition of materials subducting into Earth's interior.

1. Introduction

The seafloor is the largest boundary between the lithosphere and surface environments of the Earth, and alterations in oceanic crusts and sediments significantly influence the chemical and physical properties of the crust and the chemical composition of seawater (Alt, 2004; Demicco et al., 2005; Edmond et al., 1979). In particular, seawater penetrates basaltic crusts at mid-ocean ridges to develop hydrothermal systems. Such hydrothermal systems alter the oceanic

crust to form secondary minerals such as clay minerals and carbonates, and the evolved hot fluids are ejected from hydrothermal vents such as black smokers (Hawkesworth et al., 1979; Von Damm, 1995). The altered oceanic crust and overlying sediments eventually subduct into the Earth's interior; thus, the compositions of the subducting plate impact material recycling within the Earth's interior (Hacker, 2008; Ishikawa & Nakamura, 1994; Katayama et al., 2023; Kelley et al., 2005), and seismic activities within the subduction zones (Fujie et al., 2018; Hacker et al., 2003).

The alteration processes within the oceanic crust have been studied using several drilling projects such as the Ocean Drilling Program (ODP) and the Deep Sea Drilling Project (DSDP). Analyses of the drill cores clarified that the volcanic basement at the seafloor is extensively altered, and the extent of seafloor alteration is enhanced by rugged relief and lithological boundaries (e.g., sheet flow boundaries) and controlled by sediment blanket thickness (Alt, 2004; Alt & Teagle, 2003; Zhang & Smith-Duque, 2014). Several fluid sources for seafloor alteration have been considered: upwelling high-temperature fluid in off-axis hydrothermal circulation (Alt, 2004; Alt & Teagle, 2003; Laureijs et al., 2021; Shipboard Scientific Party, 2000), oxidizing seawater (Alt, 2004; Shipboard Scientific Party, 2011b, 2011c, 2011d; Zhang & Smith-Duque, 2014), and reduced fluid evolved by restricted seawater circulation under the sediment blanket (Alt, 2004; Alt & Teagle, 2003). As a result of this alteration, characteristic secondary minerals are produced, such as celadonite, Fe-oxyhydroxide, saponite, pyrite, carbonate, and zeolites, which can depend on the fluid sources and temperature (Alt, 2004). However, many of these secondary minerals repeatedly form under various fluid and environmental conditions, making it challenging to quantitatively evaluate and characterize seafloor alterations based solely on mineralogical descriptions.

The bulk compositions of oceanic crusts differ significantly from those of typical mid-ocean ridge basalt (MORB) during seafloor alteration (Kelley et al., 2003). This, in turn, indicates that the summation of element transfer with seafloor alteration is recorded as the change in the bulk composition, such as the addition or removal from the protolith fresh basalt composition. For example, observations of core samples suggest that an increase in alkali element concentrations (such as Rb and Cs) correlates with the formation of secondary minerals (Alt, 2004). However, quantitative distinguishment the altered bulk composition from the protolith composition remains challenging; most bulk composition analyses of altered volcanic basements required qualitative interpretation (Alt et al., 1996; Bebout, 2007; Kelley et al., 2003; Staudigel et al., 1996; Zhang & Smith-Duque, 2014).

Several previous studies on element transfer have defined the protolith composition from "fresh" volcanic glass (Kelley et al., 2003) or "fresh basalt" (Alt, 2004; Alt & Teagle, 2003; Zhang & Smith-Duque, 2014) determined from visual inspections. However, the number of unaltered samples per drilling site is limited, and it is not always clear whether the altered rocks at each site have the same protolith composition. In other words, for element transfer analyses, the protolith must be determined for individual samples, which presents a major obstacle in comparing various samples taken from different localities.

Machine learning approaches have recently been applied in the field of geochemistry, especially for classification problems such as distinguishing tsunami deposits and basalt types (Kuwatani et al., 2014; Nakamura, 2023; Ueki et al., 2018). Additionally, some studies have formulated regression problems to quantify the protolith composition from altered sample compositions. The models learn the concentration correlations among various elements in a

certain dataset (i.e., a global basalt dataset) by adopting algorithms such as decision trees (Matsuno et al., 2022) and artificial neural networks (Trépanier et al., 2016). Machine-learning models are designed to input the concentrations of several immobile elements and output the concentrations of other elements. By applying this method to the altered basalt samples, we can determine the protolith composition for each altered sample. In particular, protolith reconstruction models (PRMs, (Matsuno et al., 2022)) succeeded in reconstructing the element transfer of a typical metabasalt sample; thus, the application of this method to a set of seafloor altered basalt samples is useful for quantifying regional-scale element transfer.

In this study, we applied PRMs to altered basalts to drill core samples to clarify element transfer during the alteration of the oceanic crust. The bulk rock compositions of the depth-series drilling core samples were obtained from the Northwest Pacific region (Site 801) and South Pacific region (U1365, U1368), which have different ages and sediment thicknesses. We analyzed Rb, Ba, U, K, La, Ce, Pb, Sr, P, Nd, Y, Yb, and Lu and revealed significant amounts of element transfer at both sites, especially for Rb, K, Ba, U, Pb, Sr, and P. For samples from the South Pacific region, the results of element transfer analyses were compared with the occurrences of secondary minerals. Subsequently, the possible effects of environmental factors, such as age and sediment blanket, on the progress of alteration were discussed.

2. Methods

2.1 Protolith Reconstruction Models for Basalt

The amount of element transfer was quantified by applying a machine learning-based approach, PRMs for metabasalt (Matsuno, 2023; Matsuno et al., 2022). The PRMs enabled us to quantify the composition of the protolith basalt (i.e., original, unaltered basalt) from the metabasalt composition and quantify the amount of element transfer. The machine learning models in the PRMs were constructed by learning a composition dataset of basalt taken from PetDB (https://search.earthchem.org/), and the adopted algorithm was a gradient boosting decision tree (LightGBM, (Ke et al., 2017)). Each PRM was designed to estimate the concentration of each output element in the basalt sample of interest using the concentrations of the input elements in the same sample. In practical applications, immobile elements within the altered/metamorphosed basalt composition serve as indicative of the protolith composition and are input into the PRMs. These PRMs, trained on a basalt dataset, then estimate the protolith composition for the output elements, enabling us to calculate the quantitative element transfer using the known compositions of the protolith and altered/metamorphosed basalt. Therefore, we can quantify the protolith basalt composition of each metabasalt by utilizing the concentrations of immobile elements in the metabasalt as input data for the PRMs.

The accuracy of the PRM was assessed using the test basalt dataset, which yielded an average reproducibility ranging from 10% to 20% (Matsuno et al., 2022). By incorporating input elements such as Th, Nb, Zr, and Ti, which are typically immobile during seafloor alteration (Alt, 2004; Alt & Teagle, 2003; Kelley et al., 2003; Zhang & Smith-Duque, 2014), the coefficient of determination (R^2) between the actual concentration and the estimated concentration ranges from 0.75 to 0.95. Specifically, the R^2 value is 0.75-0.8 for Rb, K, Pb, Y, Yb, Lu, ~0.9 for Ba, U, and Sr, and greater than 0.95 for La, Ce, and Nd. This indicates that the estimation can be conducted with a high degree of reproducibility (Matsuno et al., 2022).

The PRMs were validated using a seafloor-altered basalt sample (Matsuno et al., 2022), where the protolith basalt composition was estimated by measuring the glass composition using laser ablation inductively coupled plasma mass spectrometry (LA-ICP-MS (Kelley et al., 2003)). When applying the PRMs to the compositions of the altered basalt, the estimated compositions of the protolith basalt fell within the range of the glass composition variations. Therefore, PRM is a validated quantitative method for analyzing element mobility with sufficient accuracy, even in samples where a significant element transfer has occurred.

In this study, we defined four input elements (Th, Nb, Zr, and Ti) and 13 output elements (Rb, Ba, U, K, La, Ce, Pb, Sr, P, Nd, Y, Yb, and Lu) for the PRMs. Notably, although the four input elements (Th, Nb, Zr, and Ti) are generally considered immobile during seafloor alteration, a previous study (Zhang & Smith-Duque, 2014) indicated that Th exhibits mobility. To check the rationality of the immobile elements, we scrutinized the multi-element variation diagrams for all samples and carefully checked for the absence of anomalies in the selected immobile elements. Additionally, we compared samples that were close in depth to ensure that there were no significant differences in the protolith compositions on the multi-element variation diagrams. Furthermore, we conducted a crosscheck by estimating the Th protolith composition using Nb, Zr, and Ti as immobile elements. In cases in which clear Th outliers were identified, the data for these samples were discarded. This verification process confirmed that the newly defined elements remain immobile.

Continuing, we quantified the element mobility according to the following formula:

$$M_i = \frac{C_i^{MB}}{(C_i^{PL})} \qquad (1)$$

where M_i represents the element mobility for each sample and C_i^{MB} and C_i^{PL} denote the concentrations of element i in the metabasalt sample and protolith, respectively ((Matsuno et al., 2022), Supplementary).

2.2 Compositional dataset of seafloor altered basalt

For the element transfer analyses, we selected data on the bulk rock compositions of seafloor-altered basalt samples derived from the South Pacific and Northwestern Pacific regions, courtesy of PetDB (https://search.earthchem.org/). Drilling samples from the aforementioned regions are vast. However, our analysis focused solely on specific site cores (Fig. 1): sites U1365 and U1368 from the South Pacific (Shipboard Scientific Party, 2011b, 2011d, 2011a) and site 801 from the Northwest Pacific (Shipboard Scientific Party, 1990, 2000). These sites and datasets were selected for this study because of their broad range of sampling in the depth direction (>50 m) and the use of ICP-MS for trace elements with sub-ppm concentrations. Consequently, we focused on the compositional data from the three drilling sites in terms of reliability and sufficiency.

All the original papers in the dataset were carefully checked to guarantee the precision of the PetDB dataset. We also added the sampling depth for every sample by referring to the original papers. For the South Pacific samples, we compiled the amounts of secondary minerals in each sample as reported previously (Zhang & Smith-Duque, 2014). Moreover, the thickness of the sediment layer within each site was determined based on expedition reports, facilitating the calculation of the depth from the top of the basement for every individual core. In our study, all figures utilized “depth to the basement” as the depth index, obtained by subtracting the sediment

thickness from the total depth. Data on secondary minerals for the South Pacific region have missing values for 11 samples, while compilation of compositional and sampling depth data did not have any missing values.

Some composition data were excluded from the dataset because of concerns that the elements defined as immobile may not actually be immobile, and because of doubts about measurement accuracy during sample testing. The compiled dataset was scrutinized for validity using multi-element variation and scatter plots. Anomalous samples were checked for sample descriptions and compositional data. Among the elemental groups, we paid special attention to the anomalous data for Th, Ti, and Nb. A previous study (Zhang & Smith-Duque, 2014) observed anomalies in the Th data. There is a group of samples from U1365 exhibiting advanced alteration, characterized as “Red Brown” and “Greenish Brown.” Some of these samples exhibited an obvious negative anomaly in Th in the multi-element variation diagram, and we applied the PRMs with the three input elements (Nb, Zr, and Ti). Some samples demonstrated Th leaching, including those with these specific alterations. We followed a similar procedure to examine samples from Site 801. Consequently, 11 samples (U1365: 7 samples, 801: 4 samples) were excluded from the analysis. A Ti anomaly was detected in a single sample from Site 801. This sample is described in shipboard records as containing abundant whitish clay. A Nb anomaly sample from Site 801 was confirmed by (Chen et al., 2019). The strong negative anomaly in the multi-element variation diagram might be attributed to the use of ICP-MS for Nb measurements, suggesting potential inaccuracies.

In summary, 13 samples were excluded from our analyses (multi-element variation diagrams for the excluded samples are available in the Supplementary Material). We analyzed a dataset of 201 samples, including 92 samples from Site 801, 62 samples from U1368, and 48 samples from U1365.

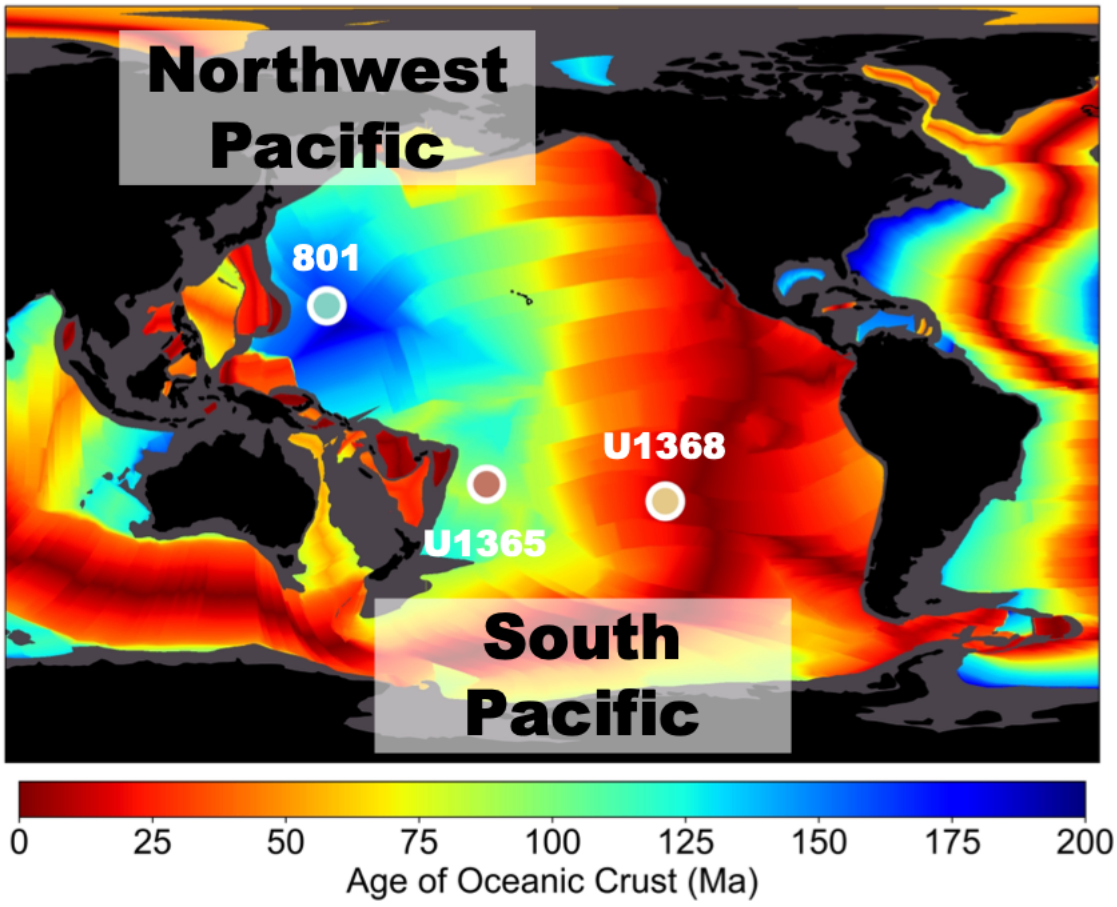

Figure 1. Location of drilling sites (Site 801, U1365, and U1368) and seafloor age map (Seton et al., 2020).

3. Geological Setting

Samples were collected from the South and Northwest Pacific regions (Fig. 1). These regions are suitable for understanding the alteration processes of seafloor basalt because they show contrasting sedimentation rates (Table 1). The average sedimentation ratio in the South Pacific is approximately 1 m/Myr, which ranks among the world's lowest (D'Hondt et al., 2009). In contrast, the Northwest Pacific region, specifically at Site 801, had a maximum sedimentation rate of approximately 32 m/Myr as the maximum (Shipboard Scientific Party, 2000).

Sediment thickness plays a pivotal role in controlling seawater flux through the sediment layer (Spinelli et al., 2004), thereby potentially influencing the chemical and hydrological environments within the basement systems. The relatively thin sediment layer in the South Pacific region results in oxidative conditions, as indicated by measurements of dissolved oxygen in the sediment layer (D'Hondt et al., 2015; Shipboard Scientific Party, 2011a, 2011c). In contrast, the thicker sediment layer in the Northwest Pacific region creates reductive conditions. A regional sample comparison focusing on different redox conditions offers insights into the alteration system depending on the redox condition.

Table 1. Average element mobility at drilling sites U1368 and U1365 in the South Pacific region and site 801 in the Northwest Pacific region.

Drilling Site Information

	Area	Latitude*	Longitude*	Age (Ma)	Sediment thickness (m)	Average sedimentation rate (m/m.y.)	Spreading rates (mm/yr)	Core length (m)	Sample number	Reference paper of Compositional Data
U1368	South	27°55.00′ S	123°09.65′ W	13.4-13.6	13.6	1.01	80 - 160	106.6	62	Zhang&Smith-Duque 2014
U1365	South	23°51.04′ S	165°38.65′ W	103.7±2.3	71	0.689	60 - 200	124.49	48	Zhang&Smith-Duque 2014
Site 801	Northwest	18°38.54′ N	156°21.59′ E	167±5 - 192±6	462	2.77	160	935.7	92	Castillo et al. 1992, Hauff et al. 2003, Kelley et al. 2003

* Describe the representative latitude and longitude here

3.1 South Pacific region

A comprehensive dataset for the composition of altered basalt was obtained from Sites U1365 and U1368 (Zhang et al., 2012, 2013; Zhang & Smith-Duque, 2014). The age of the basalt at U1365 has been reported to be 103.7±2.3 Ma, based on Re-Os dating (Zhang & Li, 2016), whereas the age of the basalt at U1368 has been reported to be 13.4-13.6 Ma, determined by magnetic polarity chron 5ABn (Shipboard Scientific Party, 2011d).

The regions where these two cores are located are well known for their low biogenic productivity and extreme oligotrophy, characterized by thin sediment layers (D'Hondt et al., 2009). Consequently, marine organic matter, which serves as an energy source for microbes, has a limited presence in the sediment layers and results in low concentrations of microbes. Typically, oxygen penetrates the marine sediments only to a depth of a few millimeters to centimeters (Revsbech et al., 1980). However, in this region, the oxygen in the seawater is almost not consumed by microbes during the penetration process due to the low abundance of marine organic matter, which leads to oxygen penetrating all the way to the seafloor throughout the depth profile of sediment layers (>50 μM) despite the presence of microbes (D'Hondt et al., 2015; Morono et al., 2020; Shipboard Scientific Party, 2011a). In addition, Fe-rich smectite is covered with microbes sustained by aerobic heterotrophy and methanotrophy (Suzuki et al., 2020). These characteristics of the South Pacific region indicate that the basalt samples taken from this area underwent alteration under oxidative conditions facilitated by the continuous inflow of seawater.

3.1.1 U1365

The U1365 basement originates from the Osbourn Trough located 250 km south of the sampling site. The Osbourn Trough is a fossil spreading center that was active during the Cretaceous period. The spreading rates of the Cretaceous Osbourn Trough were relatively fast, and ranged from 60 to 200 mm/yr (Billen & Stock, 2000; Lonsdale, 1997; Zhang et al., 2012); for the U1365 basement, the spreading rate is considered to be 140 mm/yr (Zhang et al., 2012). The protolith composition of the U1365 altered basalt is considered to range from N-MORB to

D-MORB, a variation derived from mantle-melting processes (Worthington et al., 2006; Zhang et al., 2012).

The sediment thickness at U1365 is 71 m, with an average sedimentation rate that is remarkably low at approximately 0.71 m/Myr (Shipboard Scientific Party, 2011b). The area displays a smooth relief ranging from 150 to 200 m, and U1365 is situated at a height lower than its surroundings.

Breccia fragments were rarely observed in U1365 and were recovered from two depths (Zhang & Smith-Duque, 2014). One sample was collected at a 23 m subbasement (msb) depth and was composed of mixed breccia containing basaltic and glassy clasts. The other sample was at a depth of 36 msb and was composed of basaltic breccia with calcium carbonate and hyaloclastite cement.

3.1.2 U1368

The U1368 basement originates from the Pacific-Farallon Ridge, located 300 km west of the sampling site. The spreading rates of the Pacific-Farallon Ridge ranged from ~80–85 to 160 mm/yr based on the NUVEL-1 model (Argus & Gordon, 1991; Shipboard Scientific Party, 2011d). The protolith composition of the U1365 altered basalt is considered to range from N-MORB to E-MORB (Zhang et al., 2013).

The sediment thickness at U1368 was 15 m, with a remarkably low average sedimentation rate of approximately 1.1 m/Myr. The area displays a smooth relief of less than 100 m and U1368 is situated in a more depressed area than its surroundings.

3.2 Northwest Pacific region: Site 801

Although the Northwest Pacific region includes a collection of numerous core samples through projects such as the IODP and DSDP, thorough analyses of the bulk composition along the depth axis have only been conducted for Site 801. Therefore, this study used a dataset from Site 801 as representative of the Northwest Pacific region.

Situated east of the Mariana Trench in the northwestern Pacific Ocean, Site 801 marks the initial drilling of the Jurassic Pacific Plate (Alt & Teagle, 2003; Shipboard Scientific Party, 1990, 2000). The age of the basalt was initially estimated at 167-173Ma through 40Ar-39Ar dating (Koppers et al., 2003; Pringle, 1992); however, U-Pb dating of carbonate veins within altered basalt suggests a formation age predating 192±6 Ma million years (Kendrick et al., 2022). The spreading rate at the time of formation was estimated to be 160 mm/yr (Shipboard Scientific Party, 2000). The protolith composition includes predominantly N-MORB throughout most of the core, although alkalic basalt sills intruding over the uppermost 60.2 m exhibit OIB-like compositions (Chen et al., 2019; Kelley et al., 2003; Shipboard Scientific Party, 2000).

The sediment thickness at Site 801 was 462 m. The sedimentation rate varies across units, particularly from an initial rate of 10–20 m/Myr to a later Tertiary rate of less than 1 m/Myr (Shipboard Scientific Party, 1990). A simple calculation indicates an average sedimentation rate of 2.40-2.76 m/Myr. The drilling site is located in a region with minimal topographical variation near the surface (within ±100 meters) and represents a slightly depressed area compared to its surroundings.

Lithological units were identified based on major changes in lithology and basalt mineralogy, with a significant proportion comprising subunits that include breccia. Among these units, one Breccia Unit is composed of basalt clasts at depths of 840–850 m (378-388 msb depth). This unit was interpreted to be related to tectonic activity and possible faults given its thickness of 5.0 m.

A distinguishing feature of Site 801 is the presence of yellow hydrothermal deposits and limited oxidative alteration. The intensely altered samples were recovered from depths of 521.7–531.2 m (59.7–69.2 msb depth) and 625 m (163 msb depth). Hydrothermal deposits are formed through the interaction of Si-Fe-rich low-temperature (10–100°C) hydrothermal fluids from the deep MOR spreading axis with seawater (Alt & Teagle, 2003; Shipboard Scientific Party, 2000). The most altered basalts within the core are found above and below the hydrothermal deposits, undergoing 60–100% recrystallization, whose samples are enriched with K, Rb, Ba, etc. Site 801 underwent minimal oxidative alteration compared to the other core samples, except for the hydrothermal deposit regions. The minimal oxidative alteration is attributed to the relatively flat terrain and high sedimentation rate, which restricts the influx of oxygen-containing seawater (Alt & Teagle, 2003).

3.3 Site characteristic Summary

The sites investigated in this study had spreading rates ranging from 60 to 200 mm/year, all originating from fast-spreading ridges (Table 1). Additionally, the altered basalt protolith exhibited some instances of OIB-like characteristics, but the majority was MORB. The distinctive features of each core manifest in the age of the basalt and the sedimentation rate (including sediment thickness). Through a meticulous comparison of these cores, an analysis of the alteration processes at the regional scale was conducted.

4. Visualization of Unprocessed Metabasalt Data

4.1 Compositional characteristics of the metabasalt

First, we visualized all unprocessed compositional data for each geographical area, together with sample information compiled from prior studies (Kelley et al., 2003; Shipboard Scientific Party, 2000; Zhang et al., 2012, 2013; Zhang & Smith-Duque, 2014).

Fig. 2 a, b illustrates the depth profile of Rb concentration. Rb, known to be relatively mobile with seafloor alteration (Alt, 2004; Alt & Teagle, 2003; Kelley et al., 2003; Zhang & Smith-Duque, 2014), exhibits wide variations in both regions independently from depth. Specifically, the Rb concentration remains relatively stable around 100 ppm for 801 above 60 msb depth (Fig. 2a) and 10 ppm for U1368 above 5 msb depth (Fig. 2b), whereas variations exist at other depths ranging from 0.2 ppm to 100 ppm. The heterogeneity of Rb concentration can be described as the element transfer suffering seafloor alteration, but the effects of protolith heterogeneity cannot be excluded.

In contrast, Nb and La, which are known to be relatively immobile with seafloor alteration, exhibited a relatively constant concentration at a constant depth for both regions, except for some anomalous samples (Fig. 2 c-f). Notably, the tops of U1368 (depth to basement < 5 m) and 801 (depth to basement < 50m) exhibit high concentrations of Nb and La (>10 ppm) because of the exclusive presence of OIB-like basalts in these areas (Fig. 3a, 3c; (Chen et al., 2019; Kelley et al., 2003; Zhang et al., 2012, 2013)); in contrast, the other samples exhibited

MORB-like basalt (Fig. 3b, 3d). In the depth profile of U1365, variations in concentration occurred within specific depth intervals (23 and 36 msb depth), coinciding with the presence of breccia (Fig. 2c, 2e). In contrast, for the 801 and U1368 depth profiles, the concentrations remained relatively constant (Fig. 2 c-f). The characteristic concentration profiles of Nb and La suggest that the protolith composition can vary even among samples drilled from the same site.

The contrasting depth profiles of relatively mobile and immobile elements highlights the necessity of distinguishing between the compositional information of the protolith and element transfer. The compositions of the altered basalt samples were the summation of the protolith composition and element transfer during the alteration process. Both the protolith and alteration may have variations, even within the same drilling site, and it is difficult to extract only the seafloor alteration process.

Conventional approaches for quantifying alteration include the use of a specific index (i.e., Chemical Index of Alteration (CIA)) or elemental ratio (i.e., Ba/Th). The applications of conventional approaches to the metabasalt dataset are summarized in in the supplementary information (i.e., scatter plot using elemental ratio as index, CIA distribution, the Hughes diagram).

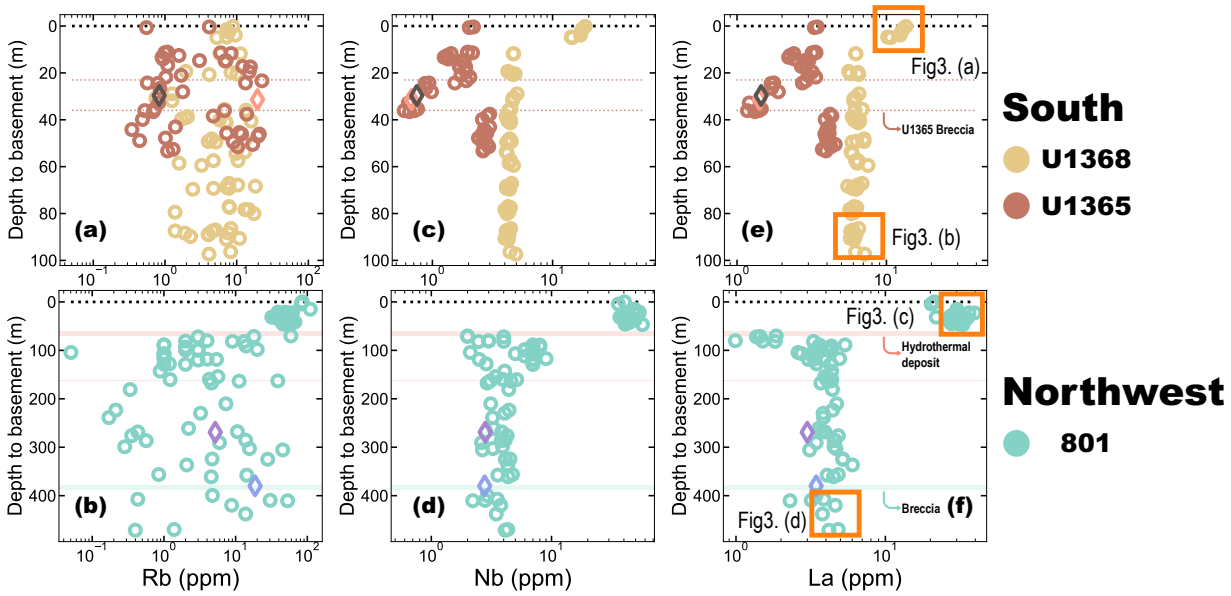

Figure 2. (**a-f**) Depth profile of the element concentration of the altered basalt in the South and Northwest Pacific regions. (a, b) Rb concentration, (c, d) Nb concentration, and (e, f) La concentration. For the profile of the South Pacific region, the dashed brown line indicates the presence of breccia in U1365. For the profile of the Northwest Pacific region, the red range highlights the presence of a hydrothermal deposit, and the light-blue range highlights the breccia unit. Depths of representative samples shown in Figure 3 are highlighted as the orange squares. Samples featured in Fig. 8 are denoted by diamond symbols in their original colors: Orange for U1365-7R-3-W0-2, dark gray for U1365-7R-1-W41-45, purple for 801C-028R-002/100-104, and dark green for 801C-040R-001/024-027.

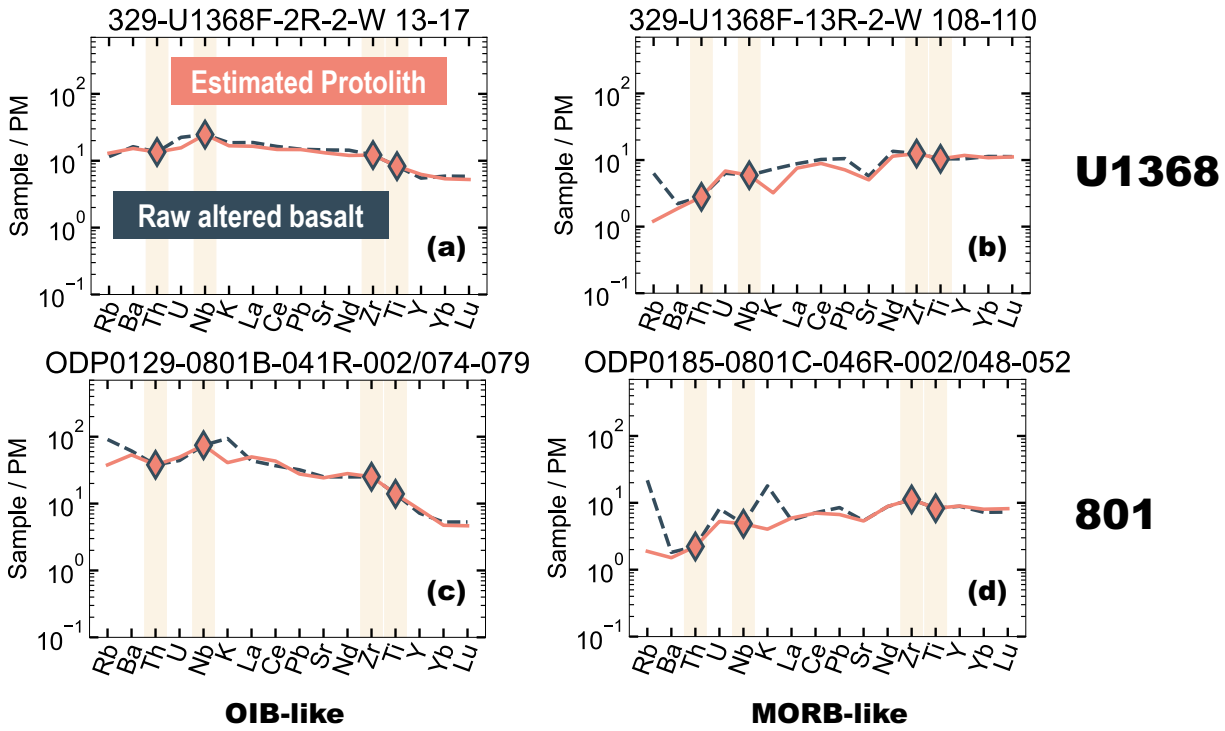

Figure 3. (**a-d**) Examples of specific depth samples displayed in primitive-mantle normalized multi-element variation diagrams. The specific depth of each sample is represented in Fig. 2. Raw altered basalt compositions are shown as a dashed dark-blue lines. Protolith compositions obtained using PRMs are shown as an orange line. Diamonds indicate input data (Th, Nb, Zr, and Ti) of PRMs.

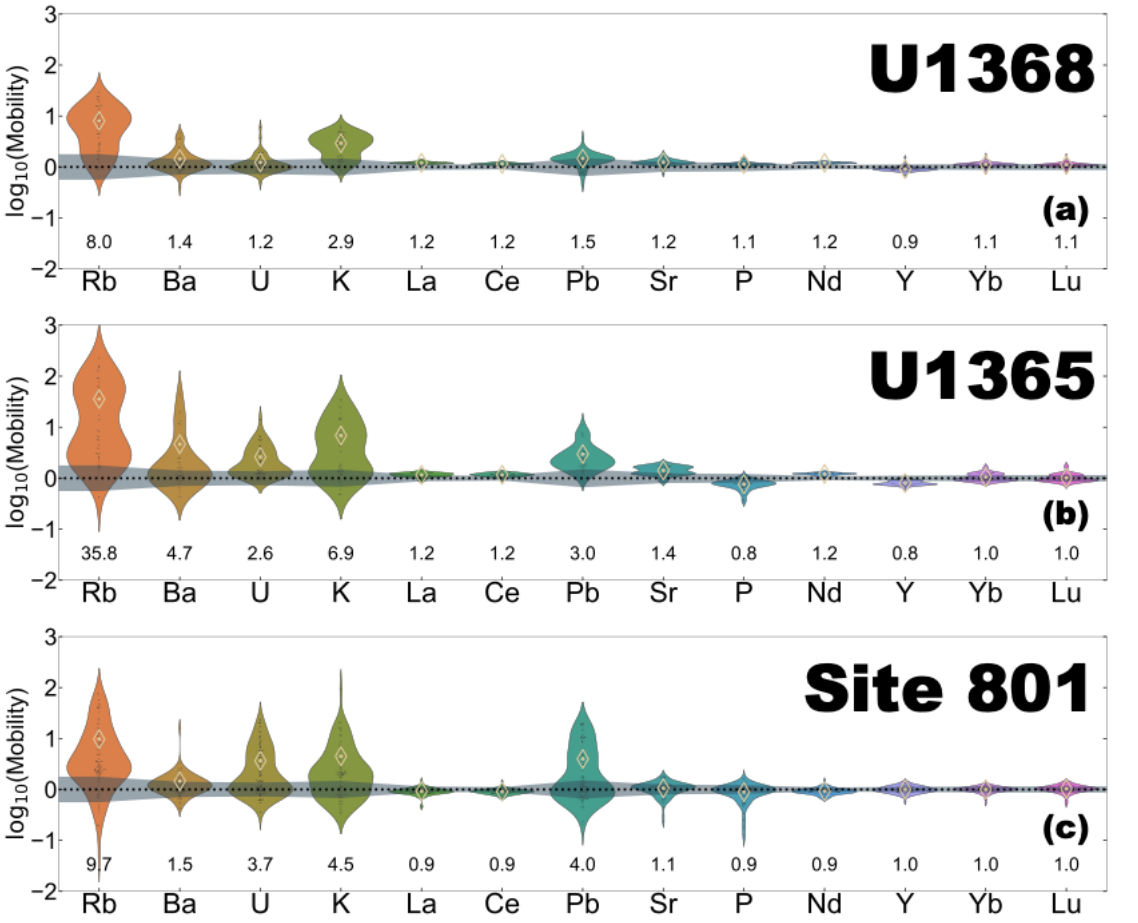

Figure 4. (**a-c**) Violin plots illustrate the frequency distribution of the estimated mobility for each element in (a) U1368 and (b) U1365, located in the South Pacific region, and (c) Site 801, located in the Northwest Pacific region. The width of the violin plots represents the kernel density estimate of the underlying distribution. The dots within each colored section denote individual data points, with the dark-blue range highlighting the reproducibility of PRMs. The average estimated mobilities for each element are denoted by diamond symbols. Additionally, the average estimated mobilities are written below each respective violin plot.

Table 2. Average element mobility at drilling sites U1368 and U1365 in the South Pacific region and site 801 in the Northwest Pacific region.

		Average Element Mobility (Altered comp. / Protolith Comp.)												
	Sample number	Rb	Ba	U	K	La	Ce	Pb	Sr	P	Nd	Y	Yb	Lu
U1368	62	8.0	1.4	1.2	2.9	1.2	1.2	1.5	1.2	1.1	1.2	0.9	1.1	1.1
U1365	48	35.8	4.7	2.6	6.9	1.2	1.2	3.0	1.4	0.8	1.2	0.8	1.0	1.0
Site 801	92	9.7	1.5	3.7	4.5	0.9	0.9	4.0	1.1	0.9	0.9	1.0	1.0	1.0

5. Result

5.1 Site Characteristic Summary

Multi-element variation diagrams (Rb, Ba, Th, U, Nb, K, La, Ce, Pb, Sr, P, Nd, Zr, Ti, Y, Yb, and Lu) were employed as illustrative examples of PRMs, focusing on samples U1368F-2R-2-W 13-17, U1368F-2R-2-108-110, 801-41R-002/074-079, and 801-46R-002/048-052 (Fig. 3 a-d). Here, we showcase selected samples that represent relatively unaltered basalt with smooth element patterns normalized by the primitive-mantle composition (Sun & McDonough, 1989). With the exception of Rb, K, and Pb, which are relatively mobile during seafloor alteration (Alt & Teagle, 2003; Kelley et al., 2003; Zhang & Smith-Duque, 2014), the estimated protolith compositions of the PRMs closely resemble those observed in the altered rocks.

Furthermore, in Fig. 3a (U1368F-2R-2-W 13-17) and 2i (801-41R-002/074-079), the protolith compositions display smooth patterns on primitive-mantle normalized multi-element variation diagrams, with elements exhibiting higher compatibility showing lower values, resembling the OIB composition. In contrast, in Fig. 3b (U1368F-2R-2-108-110) and 2j (801-46R-002/048-052), the protolith compositions resemble N-MORB-like compositions, with elements of higher compatibility having higher values. These results indicated that the protolith composition varied within the same drilling site.

Fig. 4 shows an overview of the estimated element mobilities in all sites. Across the South (Fig. 4a, b) and Northwest Pacific regions (Fig. 4c), the rages of individual element mobility show similar trends: Rb, Ba, U, K, and Pb were enriched, whereas P was depleted. The average estimated element mobility further confirmed the significant enrichment of Rb (8.0-35.7), Ba (1.4-4.7), U (1.2-3.7), and Pb (1.5-4.0) in both regions (Table 2). Additionally, when comparing the older U1365 samples to the younger U1368 samples, it was evident that the older U1365 samples displayed greater element mobility. Sr distribution was enriched in U1365 and depleted at Site 801 (Table 2). In contrast, the violin plot for elements such as La, Ce, Nd, Y, Yb, and Lu, which fall within the PRM reproducibility range, did not exhibit obvious mobility (Table 2, Fig. 4).

Based on the findings presented in Fig. 4 and Table 2, this study primarily focused on the element mobility of Rb, Ba, U, K, Pb, Sr, and P. Element transfer of Rb, Ba, U, K and Pb in both the South and Northwest Pacific regions has been reported by previous studies (Kelley et al., 2003; Zhang & Smith-Duque, 2014). These elements were also identified as mobile based on qualitative observations (Fig. 4). In contrast, elements such as La, Ce, Nd, Y, Yb, and Lu have the potential to undergo mobility with seafloor alteration and/or volcanogenic massive sulfide (Grant et al., 2020), but our results do not indicate any significant element transfer (Fig. 4).

5.1 South pacific region samples (U1365 and U1368)

Fig. 5a shows the depth profile and frequency distribution of the mobility of each element in the South Pacific region. Overall, Rb, Ba, U, K, Pb, and Sr were enriched, whereas P was depleted. Additionally, the older U1365 samples exhibited greater variation in mobility than the younger U1368 samples; however, there was no discernible trend in the depth direction for all samples except for Ba, Sr, Pb, and P. Sr gradually decreased in element enrichment, except between the two breccia depths (23 and 36 msb). In contrast, Ba, Sr, Pb, and P exhibited elemental mobility around the two breccia (23-36 msb depth).

The frequency distributions of the Rb, Ba, U, and K mobilities exhibited bimodal peaks (Fig. 5a). For Sr and Pb, bimodal peaks were only observed in the older U1365 samples, whereas for P, they were not distinct. Common to all the mentioned elements and sample sites was the presence of multimodal peaks, where one of the peaks was distributed at locations with no element mobility, whereas the other peak consistently exhibited higher element mobility in the older U1365 samples than in the U1368 samples.

The relationship between the element mobilities varied depending on the element group (Fig. 6a). The mobility of Rb and K showed a nearly linear relationship with a positive correlation ($R = 0.900$; Fig. 6a), and the slopes of the linear correlations were similar among both the older U1365 and younger U1368 samples. The mobilities of Ba, U, Pb, Sr, and P had slight or limited correlations with K, especially the U1368 samples are almost immobile for Ba, U, Pb, Sr, and P (mobility < 3 times for most samples; Fig. 6a). There are two groups of mobile elements: strongly correlated elements (i.e., Rb and K) and less correlated elements (i.e., Ba, U, Pb, Sr, and P). In addition, these two elemental groups exhibit interesting relationships. When Rb and K were enriched more than 10 times, Ba, U, Pb, and P mobility increased during enrichment/depletion compared to other samples.

5.2 Northwest pacific region samples (Site 801)

Fig. 5b shows the depth profile and distribution of element mobility in the Northwest Pacific region. Overall, Rb, U, K, and Pb were enriched, whereas P was depleted at a specific depth, and Ba was rarely enriched (mobility < 3 times). The most significant difference from the South Pacific region is that there are discernible trends with depths for Pb and P. Pb enrichment occurs exclusively at certain depths, approximately 30 ± 20 m and 100 ± 25 m, with an enrichment of up to 10 times, and P depletion was observed only at a depth of approximately 100 m. Ba enrichment was evident in samples shallower than 170 m, especially those enriched around 70 m depth, with a notable sample at around 70 m depth. In contrast, Sr depletion was confined to samples shallower than 70 m, with enrichment occurring at higher depths. For Rb, U, and K mobility, the uppermost part (~50 m) was characterized by a slightly lower amount of

enrichment/depletion than the deeper part, but enrichment was observed for widespread depth samples.

The frequency distribution of Ba exhibited only a single peak (Fig. 5b). In contrast, the frequency distributions of the mobilities of Rb, U, K, Pb, Sr, and P exhibited bimodal peaks. One of the peaks in these distributions was located near the zero elemental mobility.

The relationship between the element mobilities varied depending on the element group (Fig. 6b). The mobility trends between Rb and K were positively correlated (R=0.816; Fig. 6b). The mobilities of Ba, U, Pb, Sr, and P had slight or no correlation with K and Rb; in particular, U and Pb did not correlate at all (e.g., R=0.377 for U and K; R=0.180 for Pb and K; Fig. 6b), suggesting that the enrichment of these elements occurred independently.

5.3 Comparison of element transfer between Northwest / South pacific region

Fig. 7 shows the mobility plots of the representative element pairs between the South and Northwest Pacific regions. The Rb and K mobility trends showed remarkable similarities between the two regions, exhibiting a similar enrichment correlation. In contrast to the Rb and K mobility trends, Ba was rarely enriched (mobility < 3 times in most cases), except in one sample from the northwest region. The U and Pb mobilities for the Northwest Pacific region have trends independent of K, which are completely different from those of the South Pacific regions. Similarly, P mobility in the Northwest Pacific region showed independent depletion without K enrichment.

The samples of U1365 (South pacific region) and 801 (Northwest pacific region) have experienced seafloor alteration for approximately 1.6–1.9 times the difference in years (Table 1). However, the maximum mobility values and distributions of each element did not differ significantly. In summary, no significant differences in elemental mobility were observed between samples with different durations of seafloor alteration.

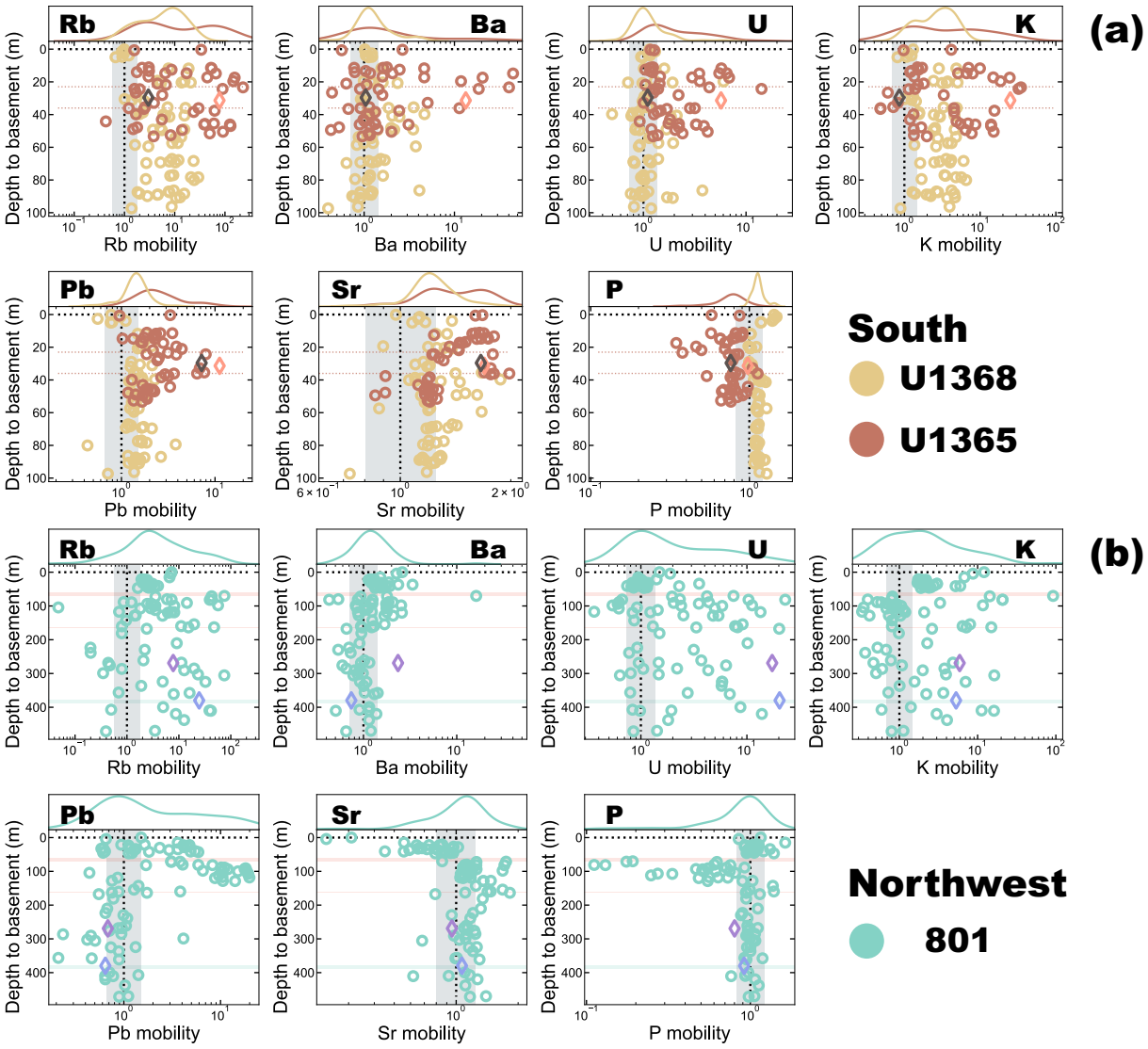

Figure 5. Depth profiles of estimated element mobility and frequency distribution for each element in two regions: (**a**) South Pacific region and (**b**) Northwest Pacific region. The Y-axis represents the depth to the basement, calculated by subtracting the sediment thickness from the total depth. Individual data points are marked as yellow dots for U1368, brown for U1365, and sky blue for Site 801, with the dark-blue range highlighting the reproducibility of PRMs. Samples featured in Fig. 8 are denoted by diamond symbols in their original colors: Orange for U1365-7R-3-W0-2, dark gray for U1365-7R-1-W41-45, purple for 801C-028R-002/100-104, and dark green for 801C-040R-001/024-027.

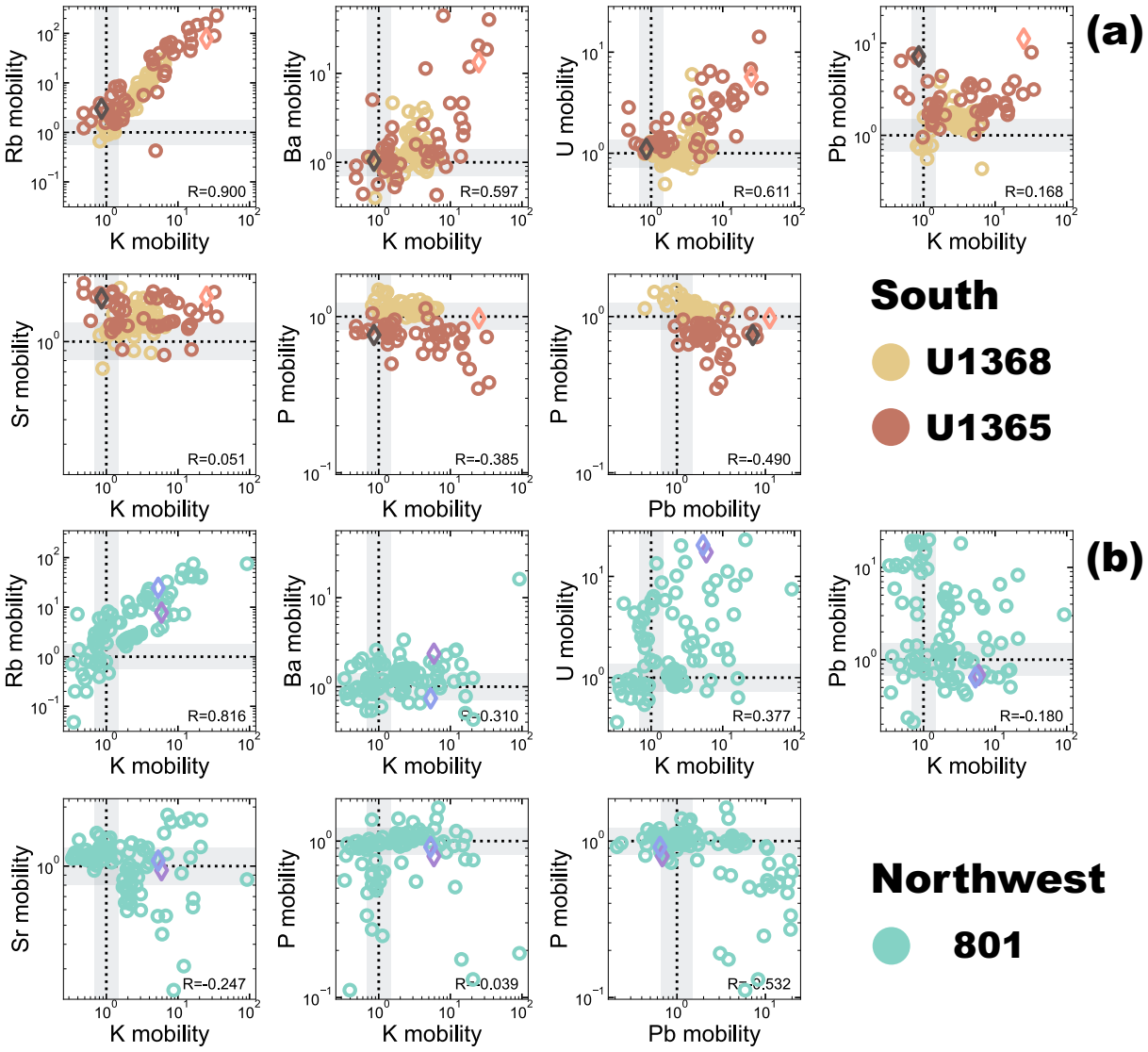

Figure 6. Relationship of element mobility in two regions: (**a**) South Pacific region and (**b**) Northwest Pacific region. The figures display the mobility relationship of K versus Rb, Ba, U, Pb, Sr, P, and Pb versus P, with correlation coefficient (R). Individual data points are marked as yellow dots for U1368, brown for U1365, and sky blue for Site 801, with the dark-blue range highlighting the reproducibility of PRMs. Samples featured in Fig. 8 are denoted by diamond symbols in their original colors: Orange for U1365-7R-3-W0-2, dark gray for U1365-7R-1-W41-45, purple for 801C-028R-002/100-104, and dark green for 801C-040R-001/024-027.

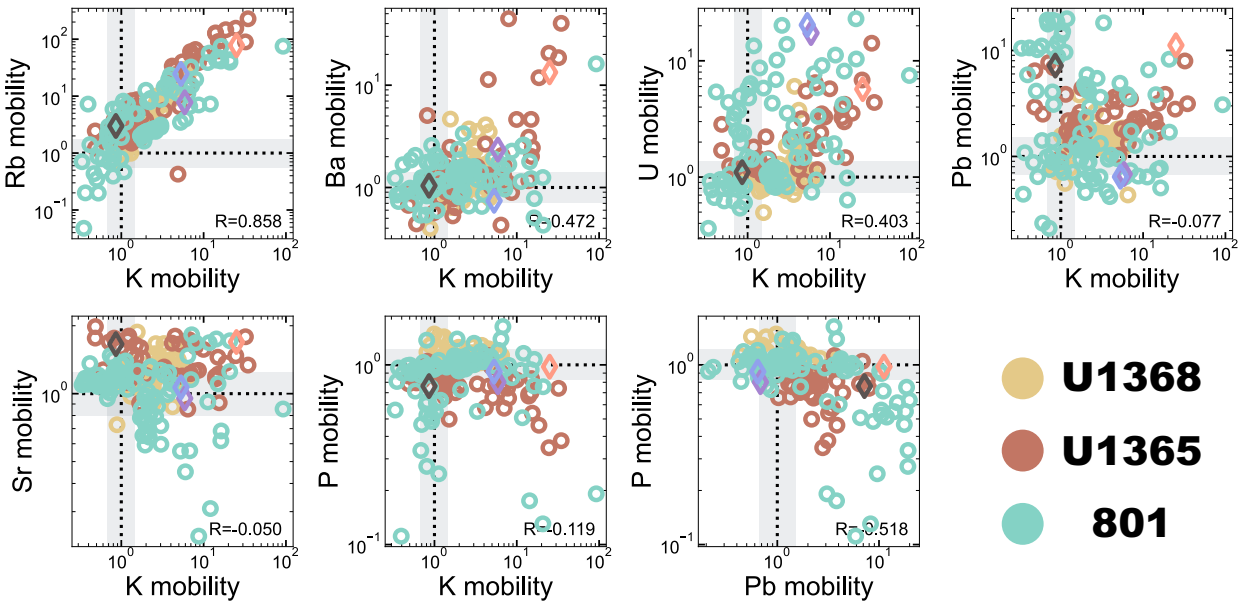

Figure 7. Relationship of element mobility in the South Pacific and Northwest Pacific regions. Figures display the mobility relationship of K versus Rb, Ba, U, Pb, Sr, P, and Pb versus P, with correlation coefficient (R). Individual data points are marked as yellow dots for U1368, brown for U1365, and sky blue for Site 801, with the dark-blue range highlighting the reproducibility of PRMs. Samples featured in Fig. 8 are denoted by diamond symbols in their original colors: Orange for U1365-7R-3-W0-2, dark gray for U1365-7R-1-W41-45, purple for 801C-028R-002/100-104, and dark green for 801C-040R-001/024-027.

6. Discussion

6.1 Enrichment with secondary alteration minerals

To understand the relationship between the types of alterations and the element transfer, we compared the estimated element mobilities of the PRMs with those of the secondary minerals. First, we compiled core image data from the Proceedings of the Integrated Ocean Drilling Program, Volumes 129 and 329. Note that core images are generally low resolution for each "distinct" sample location; we only mentioned obvious discolorations or veins when quoting the image data. Second, we compiled the mineral modes and quantitative element mobilities and comprehensively compared these values.

6.1.1 South Pacific region

6.1.1.1 Comparison with core images

The samples that exhibited enrichment in elements such as Rb, Ba, U, K, and Pb also exhibited characteristic discoloration in the core images. In particular, the sample "U1365-7R-3-W0-2" shows reddish brown discoloration in the core image (Fig. 8a) and white alteration minerals in the cores. The multi-element variation diagram of this sample showed significant enrichment in Rb, Ba, U, K, and Pb, with the Rb enrichment rate reaching up to 100 times (Fig. 6a, 8a). A similar reddish-brown discoloration is a common feature of the samples that exhibit elemental enrichment or depletion of Rb, Ba, U, K, Pb, and P.

The samples that were only enriched in Pb and depleted in P differed significantly from those mentioned above. For example, the sample "U1365E-7R-1-W 41-45" is only enriched in Pb and slightly depleted in P (Fig. 6a), as shown in the multi-element variation diagram (Fig. 8b). The core image of this sample shows no obvious discolorations.

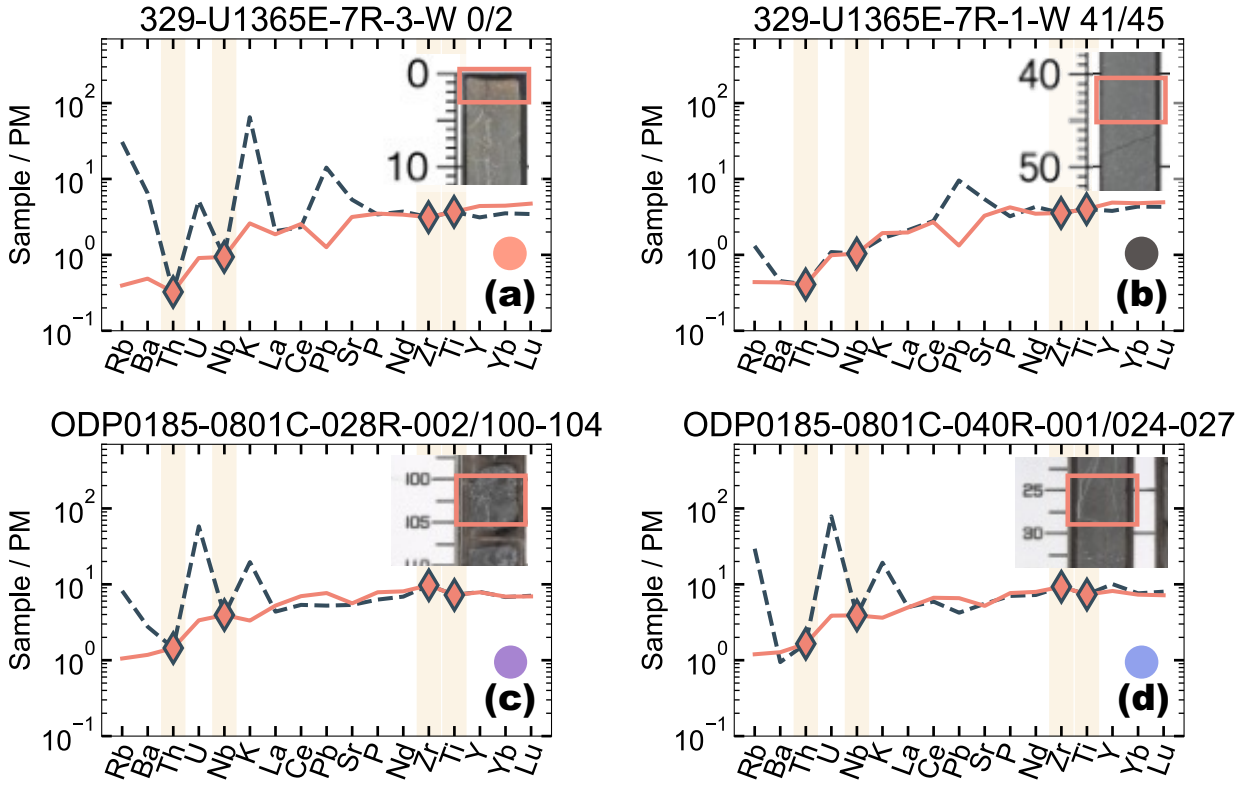

Figure 8. Examples of specific samples displayed in primitive-mantle normalized multi-element variation diagrams with core images. Raw altered basalt compositions are shown as a dashed dark-blue line. Protolith compositions obtained using PRMs are shown as a pink line. Diamonds indicate input data (Th, Nb, Zr, and Ti) of PRMs. (a) U1365-7R-3-W0-2, (b) U1365-7R-1-W41-45, (c) 801C-028R-002/100-104, (d) 801C-040R-001/024-027.

6.1.1.2 Comparison with reported secondary minerals

The mineral assemblages of U1365 and U1368 were reported previously (Zhang & Smith-Duque, 2014), based on XRD analyses. For U1365, the identified minerals include celadonite, Fe-oxyhydroxides, saponite, calcium carbonate, quartz, and sulfides, whereas for U1368, the assemblage comprises saponite, Fe-oxyhydroxides, calcium carbonate, celadonite, zeolite, quartz, and rare sulfides. In addition, a previous study reported the quantities of secondary minerals in each sample using thin sections and petrographic microscopy (Zhang & Smith-Duque, 2014). We compiled the amounts of secondary minerals in each sample and determined their relationship with the elemental mobility of the PRMs. Note that the data on secondary minerals for the South Pacific region have missing values for 11 samples (U1365: 5 samples, U1368: 6 samples).

Fig. 9 presents the relation between element mobility and mineral mode (%) of "total secondary mineral," including celadonite, saponite, Fe-oxides, carbonate, chalcedony, zeolite,

549 and quartz. The variation in the total secondary minerals in the older U1365 samples was greater
550 than that in the U1368 samples. The moderate correlation coefficients of Rb and K mobility with
551 the total secondary minerals in these samples (R = ~0.4; Fig. 9) suggested a slight correlation
552 between them. Additionally, when the secondary mineral content was particularly high (>10%),
553 the U mobility increased up to 10 times. However, no clear correlations were observed among
554 Ba, Pb, Sr, or P mobility.

555 The relationship between mobility and the amount of secondary minerals suggests that
556 Rb and K enrichment occurs concurrently with secondary mineral formation. Moreover,
557 considering the comparison with core images, Ba, U, and Pb enrichment was driven when
558 seafloor alteration was particularly advanced (Fig. 8a, 8b).

559 In the South Pacific region, the Ba, P, and Pb mobilities of the older U1365 exhibited
560 fluctuations in the depth profile, particularly around the breccia (23 and 36 msb depth; Fig. 5a).
561 Similarly, in the Northwest Pacific region, which will be discussed later, Ba, P, and Pb mobility
562 is limited to specific depths associated with hydrothermal deposits (59.7-69.2 and 163 msb
563 depth; Fig. 5b). However, as seen in the samples in Fig. 8b, while Pb is enriched, no mobility in
564 Ba and P is observed, indicating that these characteristics do not necessarily apply uniformly to
565 all samples. Consequently, the characteristic behaviors of Ba, P, and Pb were likely related to
566 local hydrothermal activity.

567 In contrast, in U1365, Sr exhibited high enrichment between the two breccias (23 and 36
568 msb depth; Fig. 5a). However, minimal enrichment was observed below the breccia and gradual
569 Sr enrichment was observed above the two breccias. The most probable explanation on the depth
570 trend of Sr is the interaction of basalt and seawater infiltrated in the vertical direction, as
571 suggested by previous studies (Kawahata et al., 1987; Krolikowska-Ciaglo et al., 2005). In
572 contrast, the U1368 samples did not exhibit gradual Sr mobility (Fig. 5a); thus, the factors
573 controlling the differences between the two hole types are not clear.

574 Altered samples from the South Pacific region with thin sediment layers indicate the
575 following (Table 3 and Fig. 10).

576 1. Enrichment of Rb and K occurred as secondary mineral formation progressed.
577 2. Ba, U, and Pb enrichment occurred when Rb and K were particularly enriched and
578 seafloor alteration was advanced.
579 3. P depletion and Ba and Pb enrichment was associated with local hydrothermal activities.
580 4. There was a possibility of gradual Sr enrichment related to inflowing seawater in the
581 vertical direction (only observed in older U1365).

582 We note that there is no clear correlation between the mobility and the amount of specific
583 secondary minerals (see Supplementary Material for details).

584

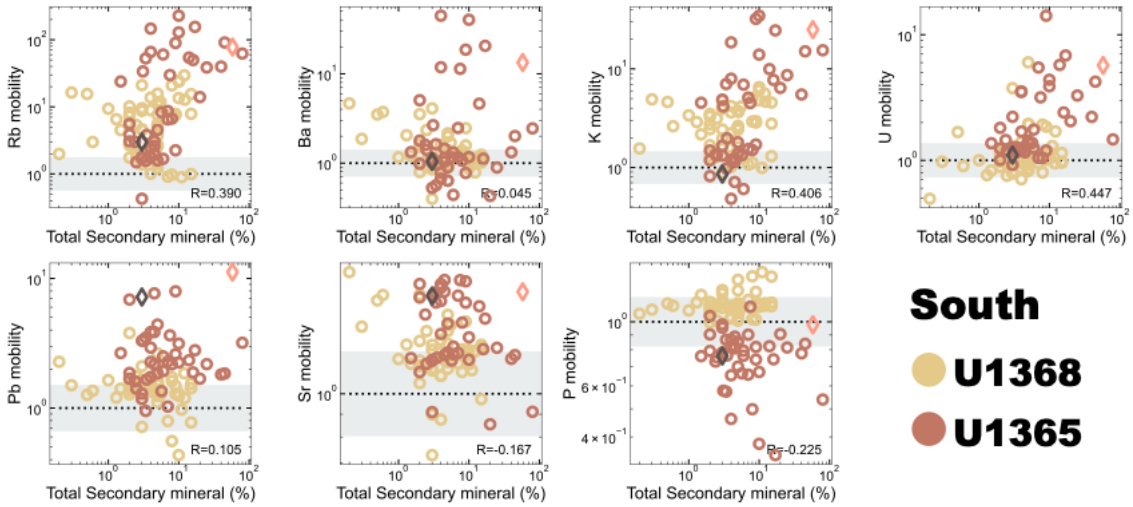

Figure 9. Relationship of total secondary mineral (%) versus the mobility of Rb, Ba, K, U, Pb, Sr, and P in the South Pacific region, with correlation coefficient (R). Individual data points are marked as yellow dots for U1368, brown for U1365, with the dark-blue range highlighting the reproducibility of PRMs. Samples featured in Fig. 8 are denoted by diamond symbols in their original colors: Orange for U1365-7R-3-W0-2, dark gray for U1365-7R-1-W41-45, purple for 801C-028R-002/100-104, and dark green for 801C-040R-001/024-027.

Table 3. Comparison of drilling site information and observed alteration events at three sites: U1368 and U1365 in the South Pacific region, and Site 801 in the Northwest Pacific region. ○: Commonly experienced, △: Occasionally experienced, ×: Not experienced.

	Drilling Site Information					Alteration Events			
	Area	Age (Ma)	Sediment thickness (m)	Sample number	Redox Condition	Secondary mineral formation progressed (+Rb, +K)	Advanced oxidative seafloor alteration (+Ba, +U, +Pb)	Hydrothermal activity (+Ba, Pb, -P)	Calcite formation in reductive cond. (+U)
U1368	South	13.4-13.6	13.6	62	Oxidative	○	×	○	×
U1365	South	103.7±2.3	71	48	Oxidative	○	○	○	△
Site 801	Northwest	167±5 - 192±6	462	92	Reductive	○	×	○	○

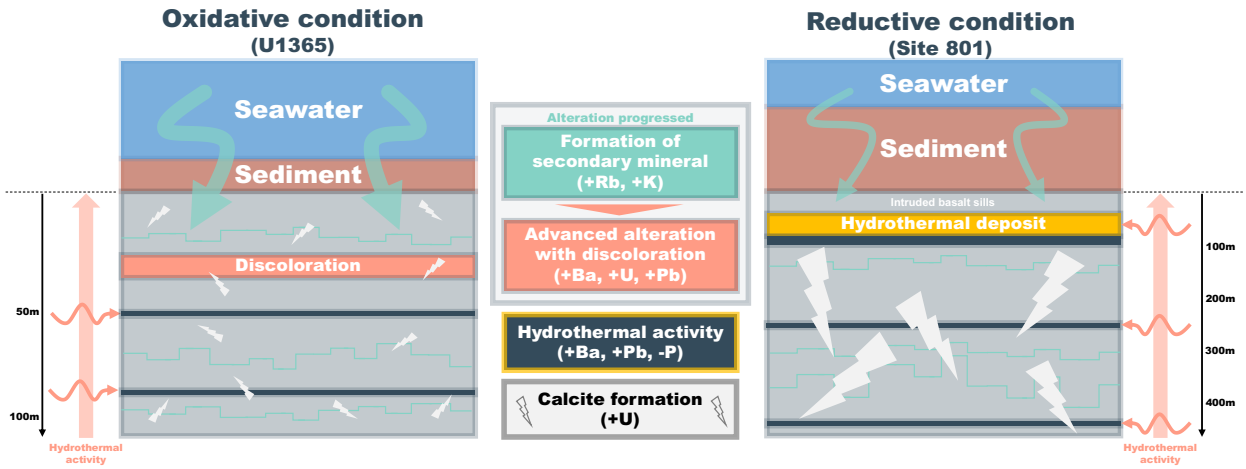

Figure 10. Schematic illustrations of seafloor alteration systems based on redox conditions, using U1365 and Site 801 as examples.

6.1.2 Northwest pacific region

The enrichment of Rb and K was associated with the formation of secondary alteration minerals, as indicated by the nearly identical trends observed in the South Pacific region (Fig. 9). However, the relationship between the core images and element mobility remains unclear. Minerals hosting Rb and K, such as celadonite and dark clay (Alt, 2004), are dark-colored minerals, making them less visible in the overall dark- and low-resolution core images (e.g., Fig. 8c and 8d). However, in Site 801 Proceedings, in addition to prominent calcite-saponite veins, dark halos consisting of dark clay were observed (Shipboard Scientific Party, 2000). This observation suggests that the enrichment of Rb and K was likely due to the formation of altered secondary minerals, similar to those in the South Pacific region.

The enrichment of U is particularly noteworthy and correlates with the characteristic core images (Fig. 8c and 8d). In the samples with concentrated U, white veins were prominently observed in the core image. These rock veins have been reported to contain alteration minerals (dark clay, calcite, smectite, celadonite veins, siliceous cement, and cherty sediments) (Shipboard Scientific Party, 2000). In addition, the presence of calcite and clay minerals within these veins indicates a potential host mineral for U (Andersen et al., 2015; Farr et al., 2001; Kelley et al., 2003). This is consistent with the relationship between element mobility and core image established in this study. The enrichment of U, accompanied by white veins, at Site 801 was observed at various depths but did not correlate with other elements (Fig. 6b ; i.e., alkali elements). This result is consistent with the findings of (Kelley et al., 2003).

Element mobility of Ba, Pb, and P observed at specific depths is associated with the formation of hydrothermal deposits (59.7-69.2 and 163 msb depth; Fig. 5b). Hydrothermal deposits at 801 are thought to form through Si-Fe precipitation from deep subsurface fluids and low-temperature hydrothermal fluids mixing with seawater (Alt & Teagle, 2003; Shipboard Scientific Party, 2000). The addition of Pb occurred within a vertical range of approximately 30–100 m in the hydrothermal deposit, whereas Ba enrichment and P depletion occurred in the lower part of the hydrothermal deposit beneath 69.2 msb depth (Fig. 5b). Core visual inspections indicate that above the hydrothermal deposit at a depth of 59.7–69.2 msb, there is a yellowish color due to Fe oxyhydroxides, whereas directly below, there is a greenish color due to smectite

(Shipboard Scientific Party, 1990). This color difference suggests the formation of secondary minerals. Thus, the alteration processes differ directly above and below hydrothermal deposits. P dissolution begins before the precipitation of Si-Fe, which leads to the formation of hydrothermal deposits, suggesting that Pb may have precipitated similarly during the formation of hydrothermal deposits.

Although the relationship between Sr and alteration minerals remains unclear from core image observations (Fig. 8c and 8d), the Sr mobility profile indicates enrichment at depths greater than 70 msb depth below the seafloor and depletion at shallower depths (Fig. 5b). Samples shallower than 70 msb depth are believed to have intruded at a later stage (Chen et al., 2019), suggesting that the alteration processes may started with different redox conditions and fluid inflows above and below the 70 msb boundary.

The deeper regions below the 70 msb may have experienced additional enrichment of Sr owing to oxidative alterations resulting from reactions with seawater, similar to those observed in the South Pacific (Fig. 5a, U1365). Conversely, in shallower regions above 70 msb depth, a reddish-brown discoloration was observed in the uppermost few meters, suggesting oxidative conditions (Shipboard Scientific Party, 1990). However, Sr depletion in these regions is inconsistent with the South Pacific. The depletion of Sr may have occurred because of alterations under conditions different from those in the South Pacific region, and further details need to be determined through a detailed sample analysis.

Based on these findings, the following processes, which are part of the South Pacific, occur in areas covered by a thick sediment layer (Table 3 and Fig. 10):

1. Rb and K enrichment with secondary minerals due to seafloor alteration.
2. At widespread depth, remarkable independent U enrichment in association with alteration mineral vein.
3. Ba and Pb enrichment/P depletion at specific depths around hydrothermal deposit.
4. Relationship between Sr enrichment/depletion and seafloor alteration remains unclear.

6.2 Governing parameters of seafloor alteration: Age and Sedimentation thickness

6.2.1 Age

Our study revealed that element mobility, especially for Rb and K, can be enriched up to 10-fold from the U1368 sample (13 Ma) to the U1365 sample (104 Ma) (Fig. 5). Greater Rb and K enrichment in the old oceanic crust was evident at Site 801 (162–192 Ma).

This study revealed the continuous progression of seafloor alteration beyond 10 Myr since the onset of alteration, as indicated by the comparison of element mobility in regional samples (Fig. 6a), which is consistent with the dating of the mineral formation, such as celadonite for 0-20 Ma under low-temperature hydrothermal fluid at the spreading axis (Laureijs et al., 2021), and calcite veins for 0-30 Ma under reducing conditions (Coogan et al., 2016; Kendrick et al., 2022). Thus, the progression of seafloor alteration continued beyond 10 Myr driven by secondary mineral formation, as element mobility recorded in bulk compositions,

669 suggesting the significant role that "age" plays a role as a parameter governing alteration
670 processes.

671 Furthermore, the frequency distribution of element mobility (Fig. 4, 5) suggests the
672 existence of a localized fluid pathway within the basaltic crust. If each alteration occurred with a
673 single alteration event and does not record multiple alteration events, the mobility peaks would
674 be similar between older U1365 and newer U1368. Additionally, if older U1365 had undergone
675 multiple alteration events and fluid pathways were newly formed for each event, it should have
676 formed a greater number of multimodal peaks. However, in the South Pacific samples, one of the
677 peaks was distributed at locations with no element mobility, whereas the other peak consistently
678 exhibited higher element mobility in the older samples (104 Ma) than in the younger samples (13
679 Ma) (Fig. 5a). Similarly, for the Northwest samples, bimodal peaks were observed in the
680 frequency distribution of the mobility (Fig. 5b). This result suggests the sporadic existence of
681 locations where fluid pathways were repeatedly utilized and others where no alteration occurred,
682 which is consistent with the observation of localized non-oxidative zones (Kurnosov et al.,
683 2008). Our findings from the frequency distribution of element mobility reinforce our
684 considerations regarding the sporadic and repeatedly utilized fluid pathway.

685 It is not yet clear when the ongoing seafloor alteration stopped after 10 Myr. Although
686 U1365 and Site 801 exhibited comparable maximum enrichment levels (Fig. 7), their ages
687 differed by nearly a factor of two, suggesting that the intense alteration at Site 801 may have
688 already stopped. However, dating of carbonate veins at Site 801 implied that the alteration was
689 still active beyond 30 Myr (Kendrick et al., 2022) and dating of other areas also exhibited
690 continuous alteration beyond 100 Myr (Wang et al., 2023). Given that carbonate formation
691 requires a restricted reducing condition covered by sediment layers (Alt, 2004), it is highly likely
692 that U1365, which contains carbonate veins, exhibited a similar or longer duration of seafloor
693 alteration than Site 801, lasting beyond 30 Myr. To obtain a more detailed understanding of the
694 duration of seafloor alteration, it is essential to measure the comprehensive bulk composition of
695 core samples (such as U1367 of ~33.5Ma located between U1365 and U1368) that fill the gap
696 within that timeframe.

697 6.2.2 Sediment thickness

698 Another key finding of this study is the variation in the mode of mineral formation due to
699 changes in alteration conditions, as reflected in the element mobility recorded in the bulk
700 compositions (Fig. 10). Sediments accumulated on oceanic plates have the potential to reduce
701 seawater inflow into the oceanic plates (Spinelli et al., 2004). As a result, seafloor alteration
702 progresses in an oxidative environment with thin sediment layers, allowing continuous seawater
703 influx, or in a reducing environment with thick sediment layers, limiting seawater penetration
704 (Alt, 2004).

705 In this study, Rb and K exhibited similar enrichment patterns (Fig. 7), indicating the
706 continuous formation of secondary minerals, regardless of the oxidative or reducing
707 environment. In oxidative environments, the enrichment of Rb and K was accompanied by the
708 mobility of Ba, U, Pb, and P as interconnected processes, forming a reddish-brown discoloration
709 and carbonate (Fig. 6a, 8a). The reddish-brown color signifies continuous alteration under
710 oxidative conditions, whereas carbonate is believed to have formed in relatively reducing
711 environments (Fig. 10). The presence of carbonate veins is rare in U1368, but is observed in
712 U1365 (Shipboard Scientific Party, 2011b, 2011d), suggesting that as the sediment thickness

increases, even at low sedimentation rates, it creates a reducing environment conducive to carbonate vein formation (Fig. 10).

In contrast, in reducing environments, most cores did not exhibit oxidative discoloration and formed carbonate veins with independent U enrichment (Fig. 8c and 8d). This is likely due to the high sedimentation rates and early-stage increases in sediment thickness, which prevented continuous oxidative alteration in the initial stages, resulting in the absence of oxidative discoloration (Fig. 10). Additionally, alterations under reducing conditions progressed, leading to the widespread formation of carbonate veins with U enrichment (Fig. 5b).

6.3 Implications for global element mobility in seafloor alteration, and caution for almost immobile elements

Based on the average element mobility data presented in Fig. 4 and Table 2, it is apparent that in oxidative environments, elements such as Rb, Ba, U, K, and Pb are significantly enriched, whereas in reductive environments, Rb, U, K, and Pb are enriched. Conversely, Sr and P did not display clear elemental mobilities on average. This suggests that oceanic-altered basalts, when serving as inputs to subduction zones, tend to undergo enrichment in Rb, K, U, Pb, and (or) Ba, on average.

The results of this study are fundamentally consistent with those of previous qualitative analyses of elemental mobility. Previous studies have noted enrichment of Rb, Ba, U, K, and Pb with seafloor alteration (Bebout, 2007; Kelley et al., 2003; Zhang & Smith-Duque, 2014), which is consistent with our findings. However, while not apparent in the averages, we unexpectedly observe a significant depletion in element mobility for Sr and P (Fig. 4, 5).

Notably, our study revealed that not all oceanic-altered basalts experience element mobility solely through alteration, and that there exists substantial variability in element mobility. This variability can be attributed to the heterogeneity of alterations along the fluid pathways. In essence, arguments based on the average may be susceptible to sampling bias, underscoring the importance of caution when utilizing the average elemental mobility values.

In this study, we focused our analysis on the transport of Rb, Ba, U, K, Pb, Sr, and P. However, we did not determine whether the other elements were completely immobile. For example, there was a slight tendency toward Nd and La enrichment (see Supplementary Materials). However, because these results were almost within the range of reproducibility of the PRMs, this study was unable to clearly indicate the element transfer for these elements. Additionally, major element transfer was not addressed in this study, leaving room for further research and analysis.

7. Conclusions

In this study, we conducted a comprehensive analysis of seafloor-altered basalt samples collected from the South and Northwest Pacific, which exhibited differences in age and sediment thickness. To quantify element mobility from bulk composition, protolith reconstruction models (PRMs) was applied to compositional data. The elemental mobility was then compared with the core images and the amount of secondary minerals. Our study is the first to report the element mobility derived from a regional dataset as follows:

The common trends were Rb and K mobilities, which exhibited a similar enrichment correlation for both regions. Among the South Pacific samples, older U1365 samples

exhibited greater enrichment in Rb, Ba, U, K, Pb, and Sr and depletion in P than younger U1368 samples. The amount of secondary minerals positively correlated with Rb and K, indicating their concurrent enrichment with secondary mineral formation. In extensively altered samples where Rb and K were particularly enriched by more than 10 times compared to the protoliths, significant element enrichment/depletion of Ba, U, Pb, and P occurred, with the progress of reddish-brown discoloration on the samples. These features of alteration and element transfer suggest the continuous penetration of oxidative seawater.

For the Northwest Pacific samples, U, Pb, and P mobilities exhibited trends different from those of Rb and K mobilities. U enrichment was observed for widespread depth samples associated with carbonate veins, whereas Pb and P mobility were observed for a certain depth related to hydrothermal deposits.

Our study suggests that the remarkable differences in element mobility governed by seafloor age and sediment thickness are as follows:

- A comparison of the older U1365 (104Ma), Site 801 (167-198Ma), and younger U1368 (13Ma) quantitatively indicates the continuous progress of seafloor alteration beyond 10 Myr since the onset of alteration. In addition, the mobility distributions of each element suggested that the fluid pathways were repeatedly utilized. The offset age of seafloor alteration could not be determined in our study; however, our mobility data and observations imply that it persisted for at least 30 Myr, irrespective of whether the environment was oxidative or reductive.
- The oxidative or reductive alteration environment is affected by the sediment thickness, which controls the inflow of seawater into oceanic basalt. Under oxidative conditions with a thin sediment thickness, the advanced mobility of Ba, U, Pb, and P was accompanied by the enrichment of Rb and K with the formation of reddish-brown discoloration and carbonate. The reddish-brown color indicates continuous alteration under oxidative conditions. In contrast, in reducing environments, most cores did not exhibit oxidative discoloration and formed carbonate veins with independent U enrichment.

Acknowledgments

This study was financially supported in part by JST SPRING, Grant Number JPMJSP2114, and JSPS KAKENHI Grant Number 23KJ0097 awarded to S.M., 22H05296, 22H01329, 22K18994 awarded to M.U., and 22H04932 and 22H05295 awarded to A.O. S.M. was partly funded by the International Joint Graduate Program in Earth and Environmental Sciences, Tohoku University (GP-EES). S.M., M.U., and A.O. were partly funded by the Joint Usage Research Center programs (ERI JURP) 2015-B-04, 2018-B-01, and 2021-B-01 (S.M., M.U., and A.O.) and by ERI JURP 2020-B-07 (M.U.) of the Earthquake Research Institute, University of Tokyo, Japan. We thank the members of the ERI JURP for their constructive discussions.

Open Research

Data from PetDB (https://search.earthchem.org/) and original papers were used to prepare this manuscript. The compiled data are provided in the Supplementary Dataset. The protolith

796 reconstruction models (PRMs) for basalt associated with this manuscript for estimating the
797 protolith composition have been published on GitHub
798 (https://github.com/MSrakugo/PRM_Streamlit, (Matsuno, 2023)). Figures were created using the
799 Python libraries Matplotlib and Seaborn (Hunter, 2007; Waskom, 2021).
800

801 **References**

802 Alt, J. C. (2004). Alteration of the upper oceanic crust: mineralogy, chemistry, and processes. In
803 *Hydrogeology of the Oceanic Lithosphere*. Cambridge University Press.
804 Alt, J. C., & Teagle, D. A. H. (2003). Hydrothermal alteration of upper oceanic crust formed at a
805 fast-spreading ridge: Mineral, chemical, and isotopic evidence from ODP Site 801. *Chemical*
806 *Geology*, *201*(3–4), 191–211.
807 Alt, J. C., Laverne, C., Vanko, D. A., Tartarotti, P., Teagle, D. A. H., Bach, W., et al. (1996).
808 Hydrothermal Alteration of a Section of Upper Oceanic Crust in the Eastern Equatorial Pacific:
809 A Synthesis of Results from Site 504 (DSDP Legs 69, 70, and 83, and ODP Legs 111, 137, 140,
810 and 148). *Proceedings of the Ocean Drilling Program, 148 Scientific Results*, *148*.
811 https://doi.org/10.2973/odp.proc.sr.148.159.1996
812 Andersen, M. B., Elliott, T., Freymuth, H., Sims, K. W. W., Niu, Y., & Kelley, K. A. (2015).
813 The terrestrial uranium isotope cycle. *Nature*, *517*(7534), 356–359.
814 Argus, D. F., & Gordon, R. G. (1991). No-Net-Rotation model of current plate velocities
815 incorporating plate motion model NUVEL-1. *Geophys. Res. Lett.*, *18*(11), 2039–2042.
816 Bebout, G. E. (2007). Metamorphic chemical geodynamics of subduction zones. *Earth and*
817 *Planetary Science Letters*, *260*(3–4), 373–393.
818 Billen, M. I., & Stock, J. (2000). Morphology and origin of the Osbourn trough. *Journal of*

819 *Geophysical Research*, *105*(B6), 13481–13489.
820 Chen, S. S., Liu, J. qi, & Lee, S. G. (2019). Mineral and geochemical characteristics for Jurassic
821 volcanic rocks from ODP Site 801C in the Pigafetta Basin, Western Pacific Ocean: Implications
822 for magmatic evolution at the oldest fast-spreading ridge. *Journal of Volcanology and*
823 *Geothermal Research*, *383*, 112–127.
824 Coogan, L. A., Parrish, R. R., & Roberts, N. M. W. (2016). Early hydrothermal carbon uptake by
825 the upper oceanic crust: Insight from in situ U-Pb dating. *Geology*, *44*(2), 147–150.
826 Demicco, R. V., Lowenstein, T. K., Hardie, L. A., & Spencer, R. J. (2005). Model of seawater
827 composition for the Phanerozoic. *Geology*, *33*(11), 877–880.
828 D'Hondt, S., Spivack, A. J., Pockalny, R., Ferdelman, T. G., Fischer, J. P., Kallmeyer, J., et al.
829 (2009). Subseafloor sedimentary life in the South Pacific Gyre. *Proceedings of the National*
830 *Academy of Sciences*, *106*(28), 11651–11656.
831 D'Hondt, S., Inagaki, F., Zarikian, C. A., Abrams, L. J., Dubois, N., Engelhardt, T., et al. (2015).
832 Presence of oxygen and aerobic communities from sea floor to basement in deep-sea sediments.
833 *Nature Geoscience*, *8*(4), 299–304.
834 Edmond, J. M., Measures, C., McDuff, R. E., Chan, L. H., Collier, R., Grant, B., et al. (1979).
835 Ridge crest hydrothermal activity and the balances of the major and minor elements in the ocean:
836 The Galapagos data. *Earth and Planetary Science Letters*, *46*(1), 1–18.
837 Farr, L. C., Plank, T., Kelley, K., & Alt, J. C. (2001). U Mineral Hosts and Enrichment Processes
838 in Altered Oceanic Crust (Vol. 2001, pp. T22C-0926). Presented at the American Geophysical
839 Union, Fall Meeting 2001, ui.adsabs.harvard.edu.
840 Fujie, G., Kodaira, S., Kaiho, Y., Yamamoto, Y., Takahashi, T., Miura, S., & Yamada, T. (2018).
841 Controlling factor of incoming plate hydration at the north-western Pacific margin. *Nature*

Communications, *9*(1). https://doi.org/10.1038/s41467-018-06320-z

Grant, H. L. J., Hannington, M. D., Hardardóttir, V., Fuchs, S. H., & Schumann, D. (2020). Trace metal distributions in sulfide scales of the seawater-dominated Reykjanes geothermal system: Constraints on sub-seafloor hydrothermal mineralizing processes and metal fluxes. *Ore Geology Reviews*, *116*, 103145.

Hacker, B. R. (2008). H2O subduction beyond arcs. *Geochemistry, Geophysics, Geosystems*, *9*(3). https://doi.org/10.1029/2007GC001707

Hacker, B. R., Peacock, S. M., Abers, G. A., & Holloway, S. D. (2003). Subduction factory 2. Are intermediate-depth earthquakes in subducting slabs linked to metamorphic dehydration reactions? *Journal of Geophysical Research, [Solid Earth]*, *108*(B1). https://doi.org/10.1029/2001jb001129

Hawkesworth, C. J., Norry, M. J., Roddick, J. C., & Vollmer, R. (1979). 143Nd/144Nd and 87Sr/86Sr ratios from the Azores and their significance in LIL-element enriched mantle. *Nature*, *280*(5717), 28–31.

Hunter, J. D. (2007). Matplotlib: A 2D Graphics Environment. *Computing in Science & Engineering*, *9*(3), 90–95.

Ishikawa, T., & Nakamura, E. (1994). Origin of the slab component in arc lavas from across-arc variation of B and Pb isotopes. *Nature*, *370*(6486), 205–208.

Katayama, I., Okazaki, K., & Okamoto, A. (2023). Role of mantle carbonation in trench outer-rise region in the global carbon cycle. *Island Arc*, *32*(1), e12499.

Kawahata, H., Kusakabe, M., & Kikuchi, Y. (1987). Strontium, oxygen, and hydrogen isotope geochemistry of hydrothermally altered and weathered rocks in DSDP Hole 504B, Costa Rica Rift. *Earth and Planetary Science Letters*, *85*(4), 343–355.

865 Ke, G., Meng, Q., Finley, T., Wang, T., Chen, W., Ma, W., et al. (2017). LightGBM: A highly
866 efficient gradient boosting decision tree. *Advances in Neural Information Processing Systems*,
867 (30), 3147–3155.
868 Kelley, K. A., Plank, T., Ludden, J., & Staudigel, H. (2003). Composition of altered oceanic
869 crust at ODP Sites 801 and 1149. *Geochemistry, Geophysics, Geosystems*, *4*(6).
870 https://doi.org/10.1029/2002GC000435
871 Kelley, K. A., Plank, T., Farr, L., Ludden, J., & Staudigel, H. (2005). Subduction cycling of U,
872 Th, and Pb. *Earth and Planetary Science Letters*, *234*(3–4), 369–383.
873 Kendrick, M. A., Zhao, J., & Feng, Y. (2022). Early accretion and prolonged carbonation of the
874 Pacific Ocean's oldest crust. *Geology*, *50*(11), 1270–1275.
875 Koppers, A. A. P., Staudigel, H., & Duncan, R. A. (2003). High-resolution40Ar/39Ar dating of
876 the oldest oceanic basement basalts in the western Pacific basin. *Geochemistry, Geophysics,*
877 *Geosystems*, *4*(11). https://doi.org/10.1029/2003gc000574
878 Krolikowska-Ciaglo, S., Hauff, F., & Hoernle, K. (2005). Sr‐Nd isotope systematics in 14‐28
879 Ma low‐temperature altered mid‐ocean ridge basalt from the Australian Antarctic
880 Discordance, Ocean Drilling Program Leg 187. *Geochemistry, Geophysics, Geosystems*, *6*(1).
881 https://doi.org/10.1029/2004gc000802
882 Kurnosov, V. B., Zolotarev, B. P., Artamonov, A. V., Lyapunov, S. M., Kashinzev, G. L.,
883 Chudaev, O. V., et al. (2008). *Technical Note: Alteration effects in the upper oceanic crust - data*
884 *and comments*. TRANSACTIONS OF THE GEOLOGICAL INSTITUTE.
885 Kuwatani, T., Nagata, K., Okada, M., Watanabe, T., Ogawa, Y., Komai, T., & Tsuchiya, N.
886 (2014). Machine-learning techniques for geochemical discrimination of 2011 Tohoku tsunami
887 deposits. *Scientific Reports*, *4*, 4–9.

888 Laureijs, C. T., Coogan, L. A., & Spence, J. (2021). In-situ Rb-Sr dating of celadonite from
889 altered upper oceanic crust using laser ablation ICP-MS/MS. *Chemical Geology*, *579*, 120339.
890 Lonsdale, P. (1997). An incomplete geologic history of the southwest Pacific basin. *Geological*
891 *Society of America. Programs with Abstracts*.
892 Matsuno, S. (2023). *Graphical Interface to Construct and Apply Machine-Learning Based*
893 *Protolith Reconstruction Models (PRMs)*. https://doi.org/10.5281/zenodo.10198882
894 Matsuno, S., Uno, M., Okamoto, A., & Tsuchiya, N. (2022). Machine-learning techniques for
895 quantifying the protolith composition and mass transfer history of metabasalt. *Scientific Reports*,
896 *12*(1), 1385.
897 Morono, Y., Ito, M., Hoshino, T., Terada, T., Hori, T., Ikehara, M., et al. (2020). Aerobic
898 microbial life persists in oxic marine sediment as old as 101.5 million years. *Nature*
899 *Communications*, *11*(1), 3626.
900 Nakamura, K. (2023). A practical approach for discriminating tectonic settings of basaltic rocks
901 using machine learning. *Applied Computing and Geosciences*, *19*, 100132.
902 Pringle, M. S. (1992). Radiometric ages of basaltic basement recovered at sites 800, 801, and
903 802, leg 129, western pacific ocean. In *Proceedings of the Ocean Drilling Program, 129*
904 *Scientific Results*. Ocean Drilling Program.
905 Revsbech, N. P., Jørgensen, B. B., & Blackburn, T. H. (1980). Oxygen in the Sea Bottom
906 Measured with a Microelectrode. *Science*, *207*(4437), 1355–1356.
907 Seton, M., Müller, R. D., Zahirovic, S., Williams, S., Wright, N. M., Cannon, J., et al. (2020). A
908 global data set of present‐day oceanic crustal age and seafloor spreading parameters.
909 *Geochemistry, Geophysics, Geosystems*, *21*(10). https://doi.org/10.1029/2020gc009214
910 Shipboard Scientific Party. (1990). Site 801. In *Proceedings of the Ocean Drilling Program, 129*

Initial Reports. Ocean Drilling Program.

Shipboard Scientific Party. (2000). Proceedings of the Ocean Drilling Program, Initial Reports, vol. 185, Ocean Drill. Program, College Station, Tex., 2000. *Proceedings of the Ocean Drilling Program, 185 Initial Reports*, *185*. https://doi.org/10.2973/odp.proc.ir.185.101.2000

Shipboard Scientific Party. (2011a). Expedition 329 summary. In *Proceedings of the IODP*. Integrated Ocean Drilling Program.

Shipboard Scientific Party. (2011b). Site U1365. In *Proceedings of the IODP*. Integrated Ocean Drilling Program.

Shipboard Scientific Party. (2011c). Site U1366. In *Proceedings of the IODP*. Integrated Ocean Drilling Program.

Shipboard Scientific Party. (2011d). Site U1368. In *Proceedings of the IODP*. Integrated Ocean Drilling Program.

Spinelli, G. A., Giambalvo, E. R., & Fisher, A. T. (2004). Sediment permeability, distribution, and influence on fluxes in oceanic basement. In *Hydrogeology of the oceanic lithosphere* (Vol. 1, pp. 151–188). https://www.researchgate.net/publication/251801278_Sediment_permeability_distribution_and_influence_on_fluxes_in_oceanic_basement/link/0a85e534d594c40e59000000/download: Cambridge University Press.

Staudigel, H., Plank, T., White, B., & Schmincke, H. U. (1996). Geochemical fluxes during seafloor alteration of the basaltic upper oceanic crust: DSDP sites 417 and 418. In *Geophysical Monograph Series* (Vol. 96, pp. 19–38).

Sun, S. S., & McDonough, W. F. (1989). Chemical and isotopic systematics of oceanic basalts: Implications for mantle composition and processes. *Geological Society Special Publication*,

42(1), 313–345.

Suzuki, Y., Yamashita, S., Kouduka, M., Ao, Y., Mukai, H., Mitsunobu, S., et al. (2020). Deep microbial proliferation at the basalt interface in 33.5–104 million-year-old oceanic crust. *Communications Biology*, *3*(1), 1–9.

Trépanier, S., Mathieu, L., Daigneault, R., & Faure, S. (2016). Precursors predicted by artificial neural networks for mass balance calculations: Quantifying hydrothermal alteration in volcanic rocks. *Computers and Geosciences*, *89*, 32–43.

Ueki, K., Hino, H., & Kuwatani, T. (2018). Geochemical discrimination and characteristics of magmatic tectonic settings: A machine-learning-based approach. *Geochemistry, Geophysics, Geosystems*, *19*(4), 1327–1347.

Von Damm, K. L. (1995). Temporal and compositional diversity in seafloor hydrothermal fluids. *Reviews of Geophysics* , *33*(S2), 1297–1305.

Wang, M., Li, H., Yang, X., Sun, W., & Chen, T. (2023). Late Pleistocene weathering and carbonation in the subduction zone oceanic basalts. *Science Bulletin of the Faculty of Agriculture, Kyushu University*.

Waskom, M. (2021). seaborn: statistical data visualization. *Journal of Open Source Software*, *6*(60), 3021.

Worthington, T. J., Hekinian, R., Stoffers, P., Kuhn, T., & Hauff, F. (2006). Osbourn Trough: Structure, geochemistry and implications of a mid-Cretaceous paleospreading ridge in the South Pacific. *Earth and Planetary Science Letters*, *245*(3–4), 685–701.

Zhang, G. L., & Li, C. (2016). Interactions of the Greater Ontong Java mantle plume component with the Osbourn Trough. *Scientific Reports*, *6*. https://doi.org/10.1038/srep37561

Zhang, G. L., & Smith-Duque, C. (2014). Seafloor basalt alteration and chemical change in the

957 ultra thinly sedimented South Pacific. *Geochemistry, Geophysics, Geosystems*, *15*(7), 3066–
958 3080.
959 Zhang, G. L., Smith-Duque, C., Tang, S., Li, H., Zarikian, C., D'Hondt, S., & Inagaki, F. (2012).
960 Geochemistry of basalts from IODP site U1365: Implications for magmatism and mantle source
961 signatures of the mid-Cretaceous Osbourn Trough. *Lithos*, *144–145*, 73–87.
962 Zhang, G. L., Chen, L. H., & Li, S. Z. (2013). Mantle dynamics and generation of a geochemical
963 mantle boundary along the East Pacific Rise - Pacific/Antarctic ridge. *Earth and Planetary*
964 *Science Letters*, *383*, 153–163.
965
966